6.4 Large-Eddy Simulations of Wake Vortices in Ground Proximity and Crosswind

Anton Stephan, Takashi Misaka, Frank Holzäpfel
Institute of Atmospheric Physics

Results from large eddy simulations of the wake vortex behaviour in ground effect with turbulent crosswinds are presented. We have conducted wall-resolved and wall-modelled simulations at different Reynolds numbers to investigate the Reynolds-number dependency. Vortex displacement and decay has been validated with experimental data. In order to understand wake vortex decay mechanisms in ground proximity the interaction of primary and secondary vortices is thoroughly investigated. Obstacles at the ground surface are introduced to trigger rapid vortex decay.

Introduction

The interaction of a two-vortex system with the ground using numerical simulations has been investigated so far with different approaches. Either wall-resolved direct numerical simulations (DNS) [2], or large eddy simulations (LES) [4] have been employed. For wall resolved simulations not only DNS but also LES is limited by the Reynolds Number, $\mathrm{Re} = \Gamma_0/\nu$, and has been realized for a maximum Re of 20000. Another possibility is to use wall-modelling functions [18], which allows considering realistic Reynolds numbers up to 10^7. Similar as [4] we have conducted wall-resolved LES at a Reynolds number of Re = 23130. Using a wall model we have further performed wall-modelled LES with Re = 231300.

In contrast to vortices at higher altitude vortex decay in ground effect is not only influenced by ambient turbulence but also by the interaction of secondary vortices detaching from the ground with the primary vortices. Here instabilities of secondary vortices play a significant roll. In contrast to the short-wavelength instability, reported in [4], we find that vortex decay is driven by the formation of omega-shaped secondary vorticity structures which themselves are triggered by the longitudinal streaks developing in the boundary layer flow close to the ground surface. Even more efficient vortex decay can be achieved by imposing dedicated obstacles at the ground plane that trigger the formation of powerful secondary vorticity structures.

In order to provide a realistic environmental flow, we first establish a three-dimensional unsteady crosswind. This way we introduce time dependent velocity fluctuations modelling the atmosphere physically. The time-averaged stream-wise velocity of the wind at the initial vortex height is set to the initial vortex descent velocity $V_0 = \Gamma_0 / 2\pi b_0$.

The presence of the ambient wind induces a boundary layer with negative vorticity. In contrast to classical considerations without wind this causes an asymmetric situation. The sudden eruption of wall vorticity is faster and more intense for the downwind vortex where the wind shear and the secondary vorticity have the same sign, but is attenuated for the upwind vortex. In the simulations temperature effects are not taken into account.

Theoretical Background

As the crosswind tends to be three-dimensional, unsteady and turbulent pre-simulations are required to generate it. Prescribing a vertical profile following the universal logarithmic law and imposing a stream-wise pressure gradient the wind flow is driven through the computational domain. In this setting the flow can be considered as a turbulent half-channel flow with the domain truncated in the middle of the channel, where a slip condition is applied. Here we shortly repeat basic properties of the channel-flow (e.g. [3], [13]). Let δ denote the channel half height and consider the following quantities as averaged in time.

For the boundary layer approximation the Navier-Stokes equations yield $\tau_w = -\delta \cdot dp/dx$, with constant pressure in wall-normal direction. The wall friction velocity is defined by $u_\tau = (\tau_w/\rho)^{1/2}$. This gives us the normalized values $u^+ = u/u_\tau \quad z^+ = zu_\tau/\nu$ and an intrinsic Reynolds number $\mathrm{Re}_\tau = u_\tau \delta/\nu$. The boundary layer of a turbulent flow has now three characteristic parts:

	region	velocity law
viscous sublayer	$z^+ < 10$	$u^+(z^+) = z^+$
transition layer	$10 < z^+ < 35$	
logarithmic layer	$35 < z^+$	$u^+(z^+) = \frac{1}{\kappa}\log(z^+) + B$,

with experimentally determined constants $\kappa = 0.41$ and $B = 5.5.$ In a fully developed flow each region has its own flow field characteristics. The viscous sublayer is shaped by coherent structures, so-called near-wall streaks (e.g. [10]). For Reynolds numbers $\mathrm{Re}_\tau < 1000$ this near-wall streaks are proven to have a spanwise spacing of $\lambda^+ \approx 100$. To resolve the viscous sublayer wall-resolved LES requires a stretched mesh in wall-normal direction, with $z^+_{\min} < 1$. For realistic Reynolds numbers this is not feasible, therefore a wall model is needed. We employ a wall model based on the logarithmic law, to establish realistic velocity profiles, also known as the Grötzbach model (e.g. [5]).

Obstacles are simulated by adding a drag force source term, $\partial u_i/\partial t = -C_D |u| u_i$, to the Navier-Stokes equations with a high drag coefficient in the region of the obstacle.

Numerical Set-up

Initial Vortex Pair

The fully rolled-up wake vortex is initialized by a pair of counter rotating Lamb-Oseen vortices. It is characterized by a circulation of $\Gamma_0 = 530$ m²/s, a vortex core radius of $r_c = 3.0$ m and a vortex separation $b_0 = 47.1$ m. The Reynolds number is set to $\mathrm{Re} = \Gamma_0/\nu = 23130$, with $\nu = 2.29 \cdot 10^{-2}$ m²/s in the wall-resolved cases and $\mathrm{Re} = \Gamma_0/\nu = 231300$, $\nu = 2.29 \cdot 10^{-3}$ m²/s in the wall-modelled case. The velocity scale is based on the initial descent velocity of the vortex pair $V_0 = \Gamma_0/2\pi b_0 = 1.79$ m/s. This defines the non-dimensional time $t^* = t\frac{V_0}{b_0}$ with b_0/V_0 = 26.3 s. For computing the initial vortex induced velocity at each point of the domain, six image vortex pairs in spanwise direction and two mirror vortices in the direction perpendicular to the ground are taken into account.

Computational Domain and Numerical Method

The dimensions of the computational domain are L_x =192 m in axial or longitudinal, L_y = 384 m in spanwise or lateral, and L_z = 144 m in vertical directions, respectively, see Figure 1. The initial height of vortex pair is set to $h_0 = b_0$. We impose periodic boundary conditions in the x and y directions. A no-slip condition is set at the ground at $z = 0$ and a slip condition at the top at $z = 3b_0$.

The number of grid points are N_x = 256, N_y = 512 and N_z = 256, resulting in 33.5 million of grid points. In the vertical direction the mesh is stretched geometrically from ground to the initial height of the vortices and remains equidistant further up.

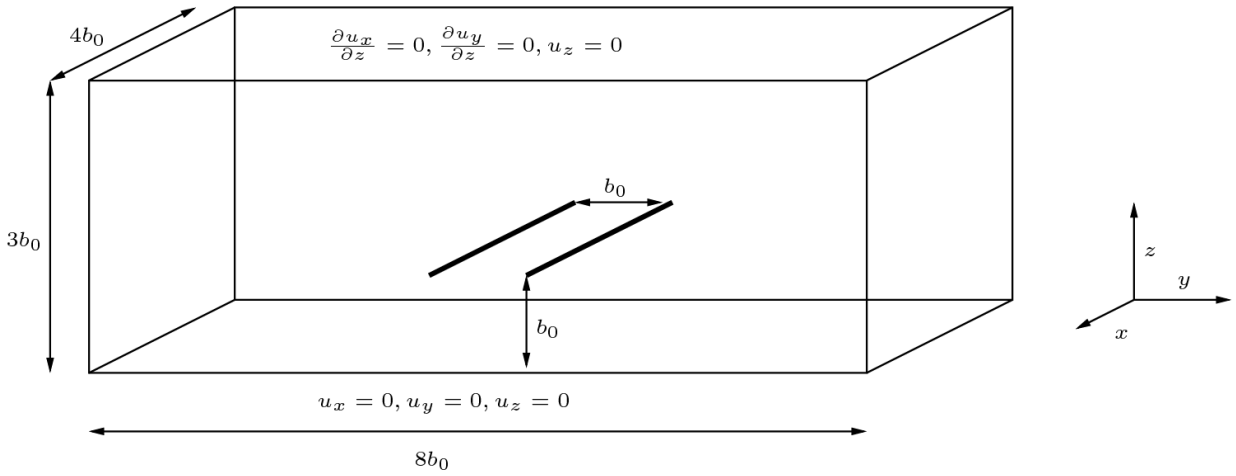

Figure 1. Sketch of the computational domain with boundary conditions and the initial vortex pair.

The mean cross-wind $u_y(z)$ is driven by a pressure gradient of dp/dy = 5.9·10^{-5} N/m^3. With a friction velocity $u_\tau = 8.414 \cdot 10^{-2}$ m/s as reference we obtain z^+_{min} = 0.55, hence, the the first layer above ground is at z_{min} = 0.15 m and we can guarantee to resolve the wall in the LES, at least for the cross-wind driven boundary layer.

We impose three different types of obstacles at the ground surface which are all oriented in the *y*-direction. The first case employs a barrier with a quadratic cross section of 9 m x 9 m; followed by a case with 3 barriers with reduced heights of 6 m and widths of 9 m separated in *x*-direction by b_0. Finally, we impose 3 sinusoidally shaped barriers (along *x*) with a height difference (two times the amplitude) of 9 m and a wave length of b_0.

The LES is performed by using the incompressible Navier-Stokes code MGLET developed at Technische Universität München [14]. The momentum equation is solved by a finite-volume approach with the fourth-order finite-volume compact scheme [12, 6]. A Lagrangian dynamical subgrid-scale model is employed [15]. The simulation is performed in parallel using 1024 processors dividing the domain into 8x16x8 parts.

Results

Flow phenomenology

When the vortex pair descends it induces a vorticity layer at the ground (see Figure 2). Crosswind also induces vorticity close to the ground, which has the opposite sign as the boundary vorticity layer of the upwind vortex and the same sign as the vorticity layer of the downwind vortex (cf. Figure 7 below). As a consequence vorticity layers generated by the wake vortices become unequally strong and the upwind and downwind vortices behave asymmetrically. The magnitude of the wake-vortex induced vorticity layer is growing leading eventually to separation and the generation of counter-rotating vortices, first at the downwind and then at the upwind vortex. Then the secondary vortices rebound and start to interact with the primary vortices, which we will discuss later in detail. We also observe a roll-up process of the turbulent structures of the wind boundary layer while these disappear at the ground between the vortices.

Trajectories and Decay

The primary and secondary vortex centres are tracked detecting local pressure minima and extreme values of vorticity. The averaged vortex core trajectories can be seen in Figure 3 together with predictions of the deterministic and probabilistic two-phase wake vortex decay and transport model (D2P, P2P) [7].

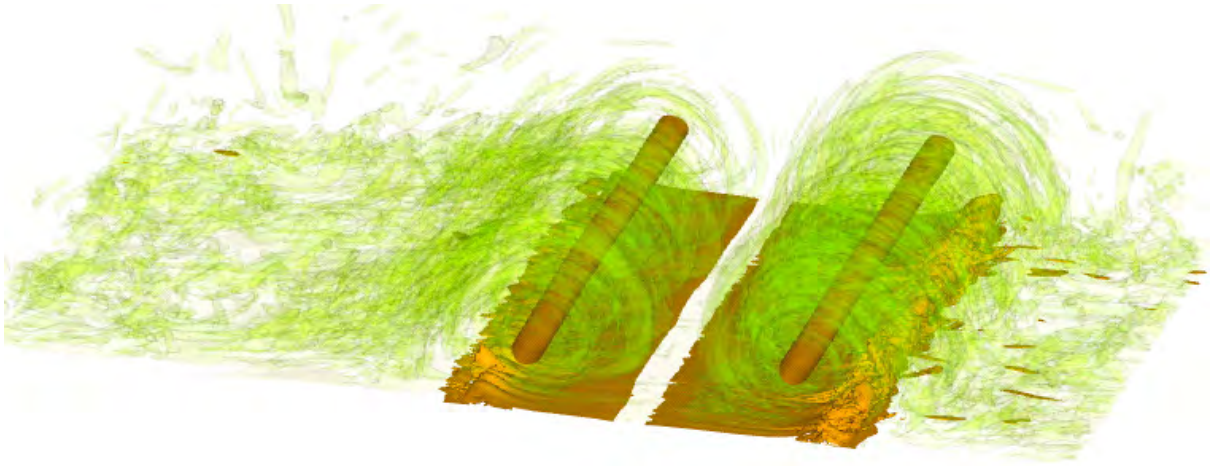

Figure 2. Visualisation of the flow field using iso-surfaces of $\|\omega\| b_0^2 / \Gamma_0 = 5$ and 0.5 at $t^* = 1.24\,\mathrm{s}$.

The averaged normalized closest distance to the ground of the primary vortices is 0.49 for the upwind and 0.57 for downwind vortex. Lidar measurements at Frankfurt airport [9] indicate average altitudes of 0.525 and 0.62, respectively, in corresponding situations [9]. Lateral displacement of the primary vortex trajectories has been analysed in [19], it scatters around a median of 3.2 at average vortex ages of t* = 3. The LES provides exactly a lateral displacement of 3.2 at a time of t* = 3.

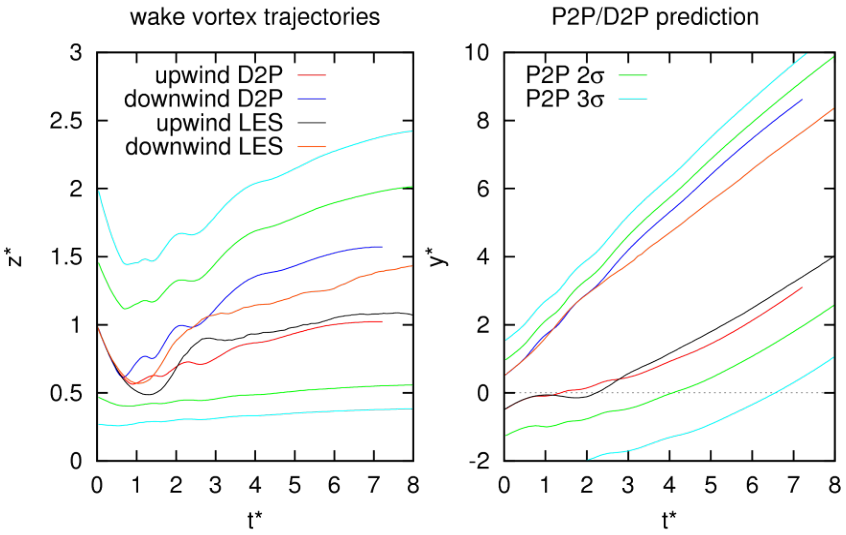

Figure 3. Evolution of normalized vertical and lateral positions. Results from simulations (black and orange) compared with predictions from D2P and P2P wake vortex model.

As a common measure of the vortex intensity for aircraft with a wingspan around 60 m we first consider $\Gamma_{5\text{-}15} = 0.1 \int_5^{15} \Gamma(r)dr$ for primary and Γ_5 for the secondary vortices, where $\Gamma(r)$ denotes the circulation distribution in a disk of radius r centred in the vortex core. The evolution of these quantities is shown in Figure 4. It is worth mentioning, that in spite of the rapid decay between t* = 1.5 and 3 the core radius of the primary vortices is shrinking temporarily, see Figure 4, right.

Wake Vortex Decay Mechanism

In contrast to the decay mechanisms away from ground, which are driven by atmospheric turbulence and thermal stratification [16], [8], the origin of turbulence in our case is the no-slip condition at the ground, i.e. the strong shear established between the free crosswind flow and the zero velocity directly at the ground surface. The counter-rotating secondary vortices finally develop into relatively strong turbulent structures causing rapid decay. Figure 5 shows how those secondary vorticity structures (SVS) develop from the ground effect vortices on both upwind and downwind vortices at different times. To our knowledge, the origin of this kind of instabilities was not well documented and explained so far.

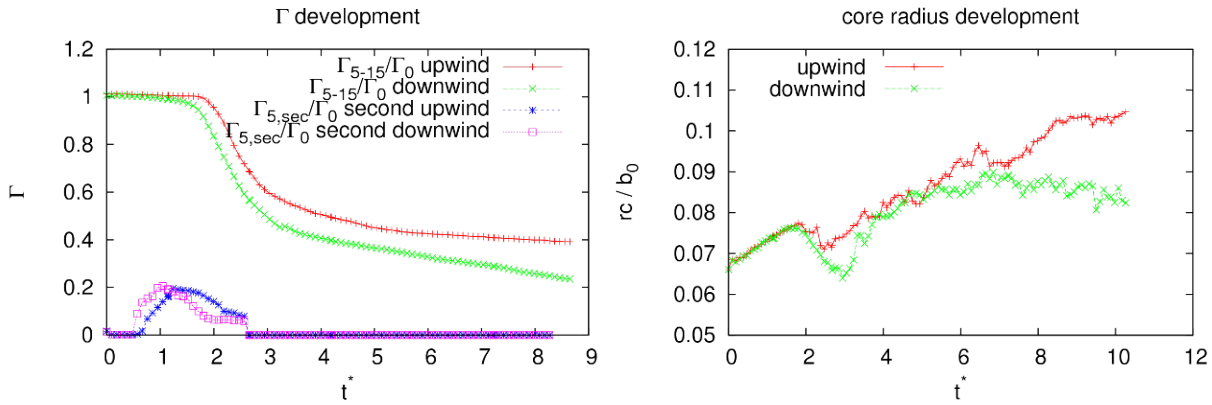

Figure 4. Evolution of vortex circulation for primary and secondary vortices (left) and core radius (right)

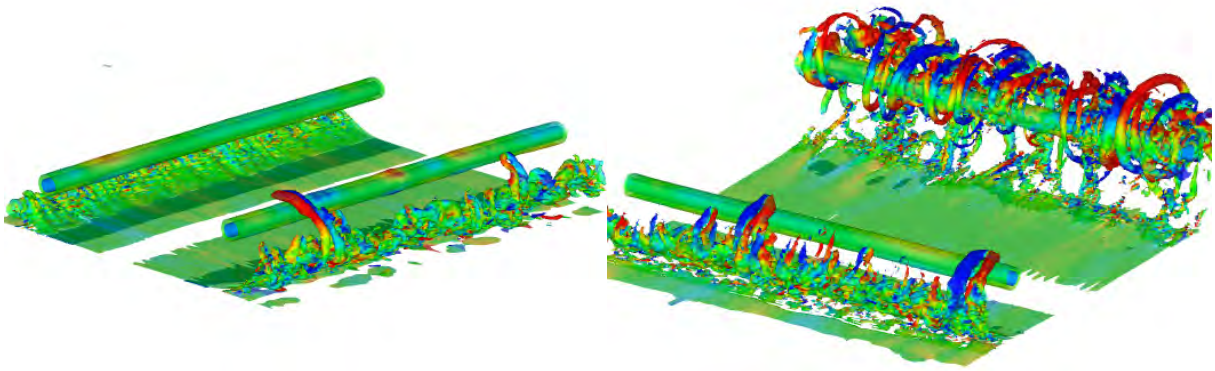

Figure 5. Iso-surfaces of vorticity magnitude $\|\omega\| = 1.5/s$, coloured by vorticity in span direction at $t^* = 1.43$ viewed upstream (left) and at $t^* = 1.81$ viewed downstream (right)

The unstable SVS wind around the primary vortex and form so-called omega loops that induce themselves a propagation speed towards the primary vortex. This self-induced approach speeds up and intensifies the interaction with the primary vortices. The prominent role of secondary vorticity structures for wake vortex decay is well known and has been analysed in detail in [8]. The formation of omega loops from secondary vortices has been studied in [17]. Here we want to focus on the origin of these instabilities.

A closer look at the velocity distribution at the ground, before imposing the vortex system reveals a wave-shaped pattern of highly elongated structures, the so-called streaks seen in Figure 6, left. These streaks correspond to regions of high velocities oriented in span direction (along u_y) in immediate ground proximity. Regions of high crosswind velocity (gradients) and low crosswind velocity (gradients) at the ground strengthen or weaken the roll-up process of the secondary vortices, respectively.

Figure 7. Sketch of flow

Crosswind velocity gradients induce vorticity of opposite sign as the secondary upwind vortex and of the same sign as the secondary downwind vortex (see Figure 7). So a region of small vertical wind gradients at the upwind secondary vortex and a region of high wind gradients at the downwind secondary vortex both enforce the secondary vortices to detach earlier, as shown in Figure 6. The shape and development of the omega loops is best visible in Figure 6 left below at the downwind vortex, whereas the correlation of the boundary layer streaks and the omega loops is even more obvious for the upwind vortex (see the red arrows in Figure 6, right).

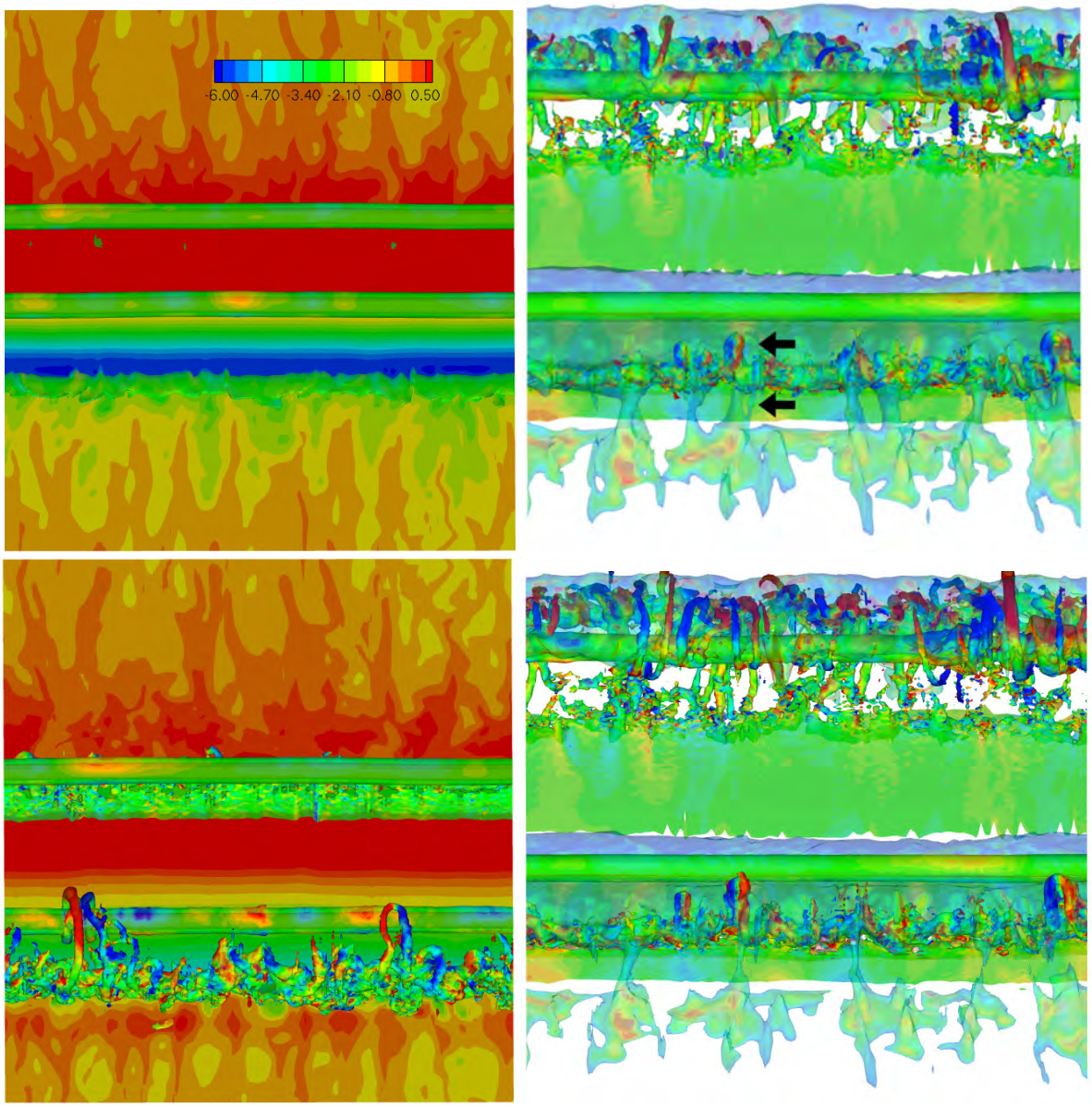

Figure 6. Iso-surface of vorticity magnitude $\|\omega\| = 1.5/s$ combined with (left) velocity at the ground at t^* = 0 (top) and 1.53 (bottom) and (right) with iso-surface of velocity v=0.1 m/s (transluscent) at t^* = 1.53 (top) and 1.81 (bottom); the lower vortex is the downwind (left) and the upwind (right) vortex.

As a consequence we may expect a one to one correspondence of the streak spacing of the crosswind flow and instability wave length of the secondary vortices. The streak spacing has found to be $\lambda^+ = 100$ in experiments ([1]) as well as in numerical simulations ([10]) for relatively small Reynolds numbers. Reference [11] gives some mathematical evidence that $\lambda^+ = 100$ may also hold for high Reynolds numbers. Consequently, the wave length of the secondary vortices is highly dependent on the Reynolds number, or in other words it is proportional to the molecular viscosity. This motivates us to perform some LES with higher Reynolds number.

Higher Reynolds Number Flows

In a simulation with $\mathrm{Re} = 231300$ and $\nu = 2.29 \cdot 10^{-3}$ m^2/s we investigate how Reynolds number affects the vortex decay. We impose a wall model based on the logarithmic wall law, to achieve the characteristic velocity profile in the pre-simulation. Again we use a pressure driven flow with the same pressure

gradient dp/dy = 5.9·10^{-5} N/m^3 as before. As expected the turbulent SVS become much smaller and are actually not too well resolved anymore, see Figure 8, left. The vortex decay at the 10 times larger Re number appears to follow the same physics but is somewhat delayed and stabilises at a slightly higher value, see Figure 8, right. This might be considered as a Re number effect but possibly could also be explained with the insufficient resolution of the turbulent structures close to the ground.

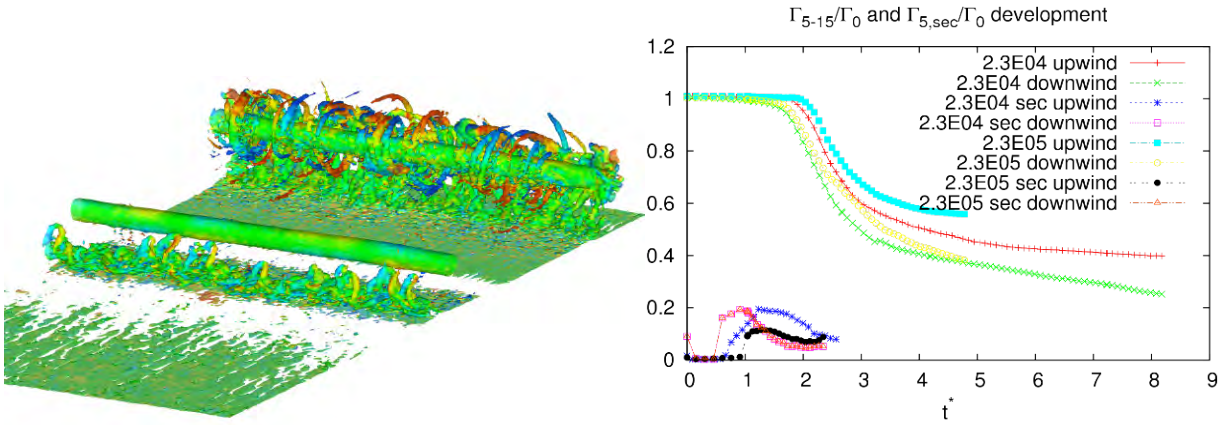

Figure 8. Left: iso-surface of vorticity magnitude $\|\omega\| = 1.5/s$, coloured by vorticity in span direction, at *t** = 1.66; right: evolution of vortex circulation for primary and secondary vortices for different values of *Re*.

Ground Obstacles

Different types of obstacles at the ground surface are introduced in order to trigger the formation of SVS and to achieve premature vortex decay. All initial parameters of the cross-wind and the wake vortices are taken from the wall-resolved LES at Re = 23130.

One barrier with quadratic cross section

After vortex initialisation secondary vorticity is generated rapidly at the top of the barrier, which subsequently detaches and develops a distinct loop, see Figure 9. The loop is stretched and winds around the primary vortex forming an omega loop, approaching and immersing into the primary vortex. The process follows the vortex stretching and tilting mechanisms explained in [8]. The geometrically induced SVS travel along the primary vortices by self-induced velocity while they weaken the primary vortices efficiently.

This simulation can be considered as a very clear illustration of the development of an SVS in the crosswind situation. While in the turbulent cross-wind situation several smaller SVS develop from the boundary layer streaks competing with less coherent turbulent structures, the obstacle (running parallel to the cross-wind direction) triggers a very distinct large single unadulterated secondary vorticity loop. Consequently, the different phases of its development can more clearly be distinguished in Figure 9.

Three barriers with different cross sections

Here we compare the influence of barriers with sinusoidal and squared cross sections. Three obstacles are imposed separated by b_0 along x. Figure 10 reveals that the flow characteristics are very similar for smooth and polygonal barriers. Both simulations show similar results concerning the evolution of the vortex intensity. All cases have in common that the geometrically induced instabilities weaken the primary vortices. In Figure11 the development of $\Gamma_{5\text{-}15}$ is plotted for all three cases with obstacles compared to the simulation with flat ground. The downwind vortices are fully decayed already between t^* = 3 and 4 compared to the pure cross-wind case where the downwind vortex survives beyond simulation time. Until t^* = 3 the upwind vortices in all three cases with obstacles show similar decay characteristics, multiple obstacles, obviously, result in lower final circulations.

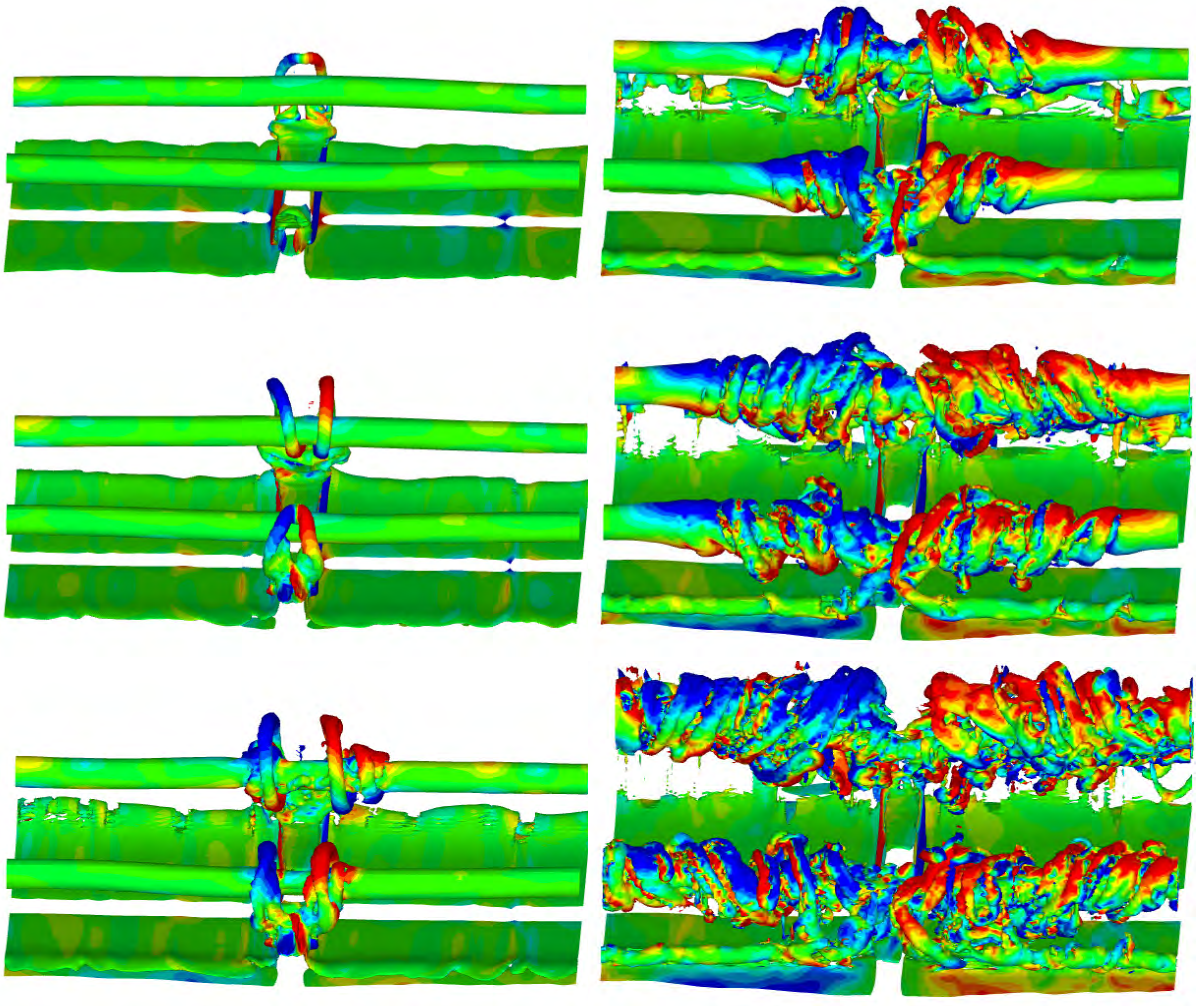

Figure 9. Iso-surface of vorticity magnitude $\|\omega\| = 1.5/s$, coloured by vorticity in span direction at t^* = 0.76, 0.91, 1.06, 1.21, 1.37, and 1.52, from top to bottom and left to right.

Conclusions

We conducted several LES to study the evolution of a counter-rotating vortex pair in ground effect with cross-wind. The investigation of the decay mechanism reveals that the strongly deforming and unstable secondary vortex structures trigger the rapid decay of the primary vortices. This motivated us to study the origin of the instabilities, which can be either initiated dynamically by coherent structures of the crosswind flow or geometrically by obstacles installed at the ground.

In the case with a flat lower boundary we found that the velocity streaks in the cross-wind flow close to the surface support the formation of secondary vorticity and thus accelerate the detachment of secondary vortices from the ground which subsequently causes the generation of omega loops. These omega loops approach the primary vortices driven by self-induced velocity and initiate the rapid decay in ground proximity.

Because the wall-resolving LES limits the Reynolds number of the flow, we further have conducted a simulation with a Re larger by a factor of 10. This forced us to model the near wall effects. The results show that the described instabilities of the secondary vortices are more filigree leading to a somewhat delayed vortex decay. Possibly, the employed wall model does not allow representing coherent small turbulent structures close to the ground with sufficient resolution.

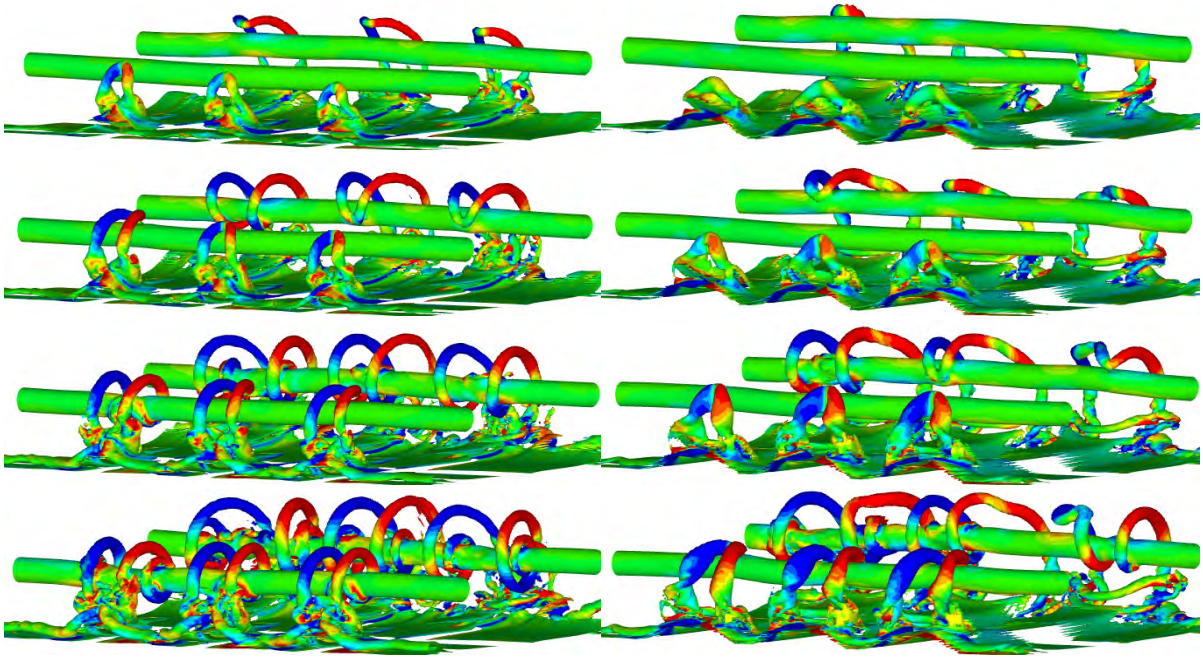

Figure 10. Iso-surface of vorticity magnitude $\|\omega\| = 1.5/s$, coloured by vorticity in span direction at *t** = 0.98, 1.06, 1.14, and 1.21. Left: square shaped barriers. Right: sinusoidal barriers.

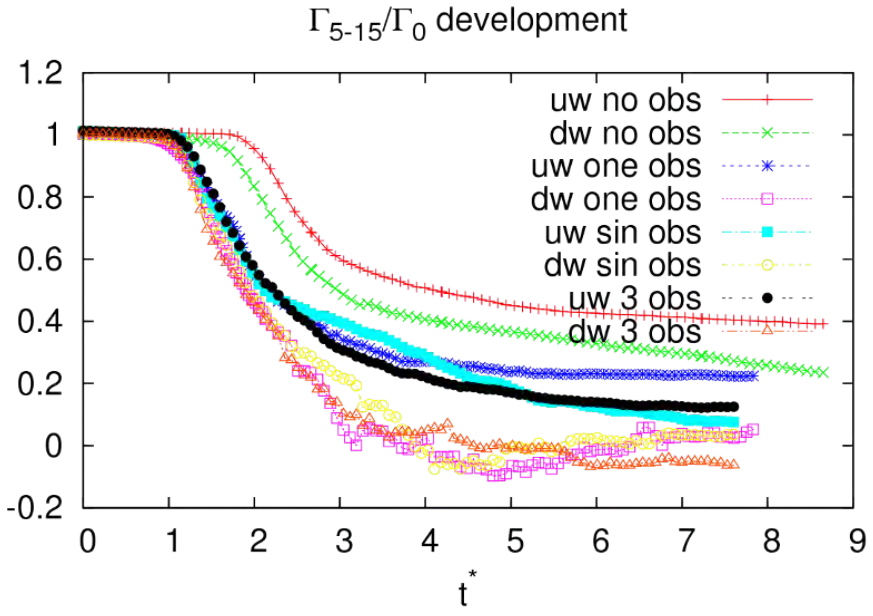

Figure 11. Evolution of vortex circulation, LES with / without obstacles; uw/dw = up-/downwind vortex.

Finally, we imposed obstacles of different type and shape. This setup allowed the dedicated use of properties of vortex dynamics to accelerate wake vortex decay in ground proximity with the following characteristics:

- early detachment of strong omega-shaped secondary vortices
- omega shape causes self-induced fast approach of the primary vortex
- after the secondary vortex has looped around the primary vortex it separates and travels along the primary vortex again driven by self induction

- the dedicated secondary vortex connects to the regular ground effect vortex and thus obtains continued supply of energy
- the highly intense interaction of primary and secondary vortices leads to rapid wake vortex decay independent from natural external disturbances

In summary the introduction of obstacles at the ground supports the selective generation of secondary vortices and smart utilisation of vortex properties in order to generate fast approaching and rapid spreading of disturbances along the primary vortex leading to premature vortex decay in ground proximity. Optimal obstacle shape and assembly with regard to vortex decay and feasibility is still to be investigated.

Acknowledgements

The simulations have been performed at DKRZ (Deutsches Klimarechenzentrum), Juropa (Forschungszentrum Jülich) and LRZ (Leibniz-Rechenzentrum). We would like to thank Andreas Dörnbrack for providing computation time at DKRZ as well as Prof. Dr. M. Manhart for providing the original version of the LES code MGLET. The work was funded by DLR project Wetter & Fliegen.

References

[1] Cantwell B., Coles D., Dimotakis P. (1978) Structure and Entrainment in the Plane of Symmetry of a Turbulent Spot, Vol. 87, 641-672.

[2] Duponcheel M., Lonfils T., Bricteux L., Winckelmans G. (2006) Simulations of three dimensional wake vortices in ground effect using a fourth-order incompressible code. 7th Nat.Congress on Theoretical and Applied Mechanics, Mons.

[3] Fröhlich J. (2006) Large Eddy Simulation turbulenter Strömungen. B.G. Teubner Verlag.

[4] Georges L., Geuzaine P., Duponchel M., Bricteux L., Lonfils T., Winckelmans G., Giovannini A. (2005) Technical Report 3.1.1-3, LES of two-vortex system in ground effect with and without wind. Techn. Ber., Université catholique de Louvain, Institut de Mécanique des Fluides de Toulouse.

[5] Grötzbach G. (1987) Direct numerical and large eddy simulation of turbulent channel flows. Encyclopedia of Fluid Mechanics (ed. N. Cheremisinoff). West Orange, NJ.

[6] Hokpunna A., Manhart M. (2010) Compact Fourth-order Finite Volume Method for Numerical Solutions of Navier-Stokes Equations on Staggered Grids. Journal of Computational Physics, Vol. 229, Nr. 20, pp. 7545-7570.

[7] Holzäpfel F. (2003) Probabilistic Two-Phase Wake Vortex Decay and Transport Model. Journal of Aircraft, Vol. 40, Nr. 2, pp. 323-331.

[8] Holzäpfel F., Hofbauer T., Darracq D., Moet H., Garnier F., Ferreira Gago C. 2003: Analysis of wake vortex decay mechanisms in the atmosphere. Aerospace Science and Technology. Vol.7, 263-275.

[9] Holzäpfel F., Steen M. (2007) Aircraft Wake-Vortex Evolution in Ground Proximity: Analysis and Parameterization. AIAA Journal, Vol. 45, 218-227.

[10] Jimenez J., Moin P. (1991) The minimal flow unit in near-wall turbulence. Journal of Fluid Mechanics Vol. 225, 213-240.

[11] Kathryn M. Butler and Brian F. Farrell 1993: Optimal perturbations and streak spacing in wall-bounded turbulent shear flow, Physics of Fluids Vol.5, 774-777.

[12] Kobayashi, M. H. (1999) On a Class of Páde Finite Volume Methods. Journal of Computational Physics, Vol. 156, Nr. 1, 137-180.

[13] Kundu P. (1990) Fluid Mechanics. Academic Press.

[14] Manhart M. (2004) A Zonal Grid Algorithm for DNS of Turbulent Boundary Layer. Computer and Fluids, Vol. 33, Nr. 3, 435-461.

[15] Meneveau C., Lund T.S., Cabot W.H. 1996: A Lagrangian dynamic subgrid-scale model of turbulence. Journal of Fluid Mechanics Vol 319, 353-385.

[16] Misaka T., Holzäpfel F., Hennemann I. Gerz T., Manhart M., Schwertfirm F. 2012: Vortex bursting and tracer transport of a counter-rotating vortex pair, Physics of Fluids, in press.

[17] Ortega J.M., Bristol R.L., Savas Ö. 2003: Experimental study of the instability of unequal strength counter-rotating vortex pairs. J. Fluid Mech., 474, 35-84.

[18] Proctor F.H., Han J.: 1999: Numerical Study of Wake Vortex Interaction with the Ground using the Terminal Area Simulation System. AIAA, 99-0754, 37th Aerospace Sciences Meeting & Exhibit, Reno.

[19] Steen M. (2005) Analyse und Parametrisierung des Wirbelschleppenverhaltens in Bodennähe. Diplomarbeit, Technische Universitaet Braunschweig.